Impact of Defocusing of the Camera Lens on the Image in Optical Camera Communications

Navid Bani Hassan[1], Yingjia Huang[1], Zhenyi Shou[1], Zabih Ghassemlooy[1,2], Stanislav Zvanovec[3], Min Zhang[4], and Xuan Tang[2]

[1]Optical Communications Research Group, Northumbria University, Newcastle-upon-Tyne, UK
[2]QIEM, Chinese Academy of Sciences, Fujian, China
[3]Department of Electromagnetic Field, Czech Technical University in Prague, Technicka 2, 16627 Prague, Czech Republic
[4]State Key Laboratory of Information Photonics and Optical Communications, Beijing Univ. of Posts & Telecom, Beijing, China
Emails: {navid.hassan, yingjia.huang, zhenyi.shou, z.ghassemlooy}@northumbria.ac.uk, xzvanove@fel.cvut.cz, mzhang@bupt.edu.cn

***Abstract*—In this paper, we propose a theoretical model for the intensity of a blurred image of a light source (LS) due to defocusing in optical camera communications. The blurred image is characterized with four parameters of half power full width, maximum intensity, left and right slope of hazy area and we relate them to the LS, channel, and camera settings. We experimentally investigate the impact of these parameters on characterization of the blurred image and compare it with the predicted data. The results show that if the size of the LS compared to its distance from the camera is less than a certain value set by the camera settings, the interference level between two close LSs increases, i.e. by increasing the link span, the size of the image increases.**

Keywords—optical camera communications; defocusing;

I. INTRODUCTION

Recent developments in light emitting diodes (LEDs) as efficient light sources (LSs) have made them popular for both lighting and data communications purposes. LEDs with high switching speeds up to 20 MHz are the prominent candidates for optical wireless communications in particular visible light communications (VLC) [1]. Availability of LED based lighting fixtures in indoor and outdoor environments, low energy consumption, low costs, license free and a full-duplex communications mode are the key features of LED-based VLC [2]. In addition LEDs and laser diodes (LDs) used in many applications including vehicles head- and tail- lights, inside plane and trains etc., which could be exploited as part of intelligent transport system (ITS). Line of sight (LOS) based VLC systems employing LEDs and photodiodes (PDs) have been widely investigated. However, such systems suffer from blocking and shadowing and offer limited mobility, which could be a serious issue in car-to-car (C2C) communications. These problems could be addressed by employing an image sensors (ISs) used in typical cameras, which offer improved mobility are more tolerant to shadowing [3, 4]. This is due to availability of a large number of photodiodes in the IS, thus offering massive multi-input multi-output (MIMO) with spatial diversity [5]. Note that, camera-based VLC systems offer vision, localization, range measurements and data communications [2, 6-9]. Hence, optical camera communications (OCC) being a viable option in C2C communication.

Current commercial cameras can record videos of up to 960 frame per second (fps) for a smartphone [10] and up to 1 Mfps for a camera recorder [11]. The camera's frame rate set the upper limit for data transmission in OCC. In C2C communications the main purpose to send and received traffic safety information, which is very low (i.e., < 1 kbps), therefore low fps based camera can effectively be used. However, lower fps will lead to flickering, which were addressed in [12] and [13]. Additionally, there are other challenges including (*i*) detection and tracking of LSs in the image, where a number of algorithms have been proposed [4, 14, 15]; and (*ii*) blurry image due to LSs seen by the camera being out of focus, thus may lead interference.

In this paper, we investigate the impact of different parameters of LSs, channel and camera on the characterization of the LS image. We propose a theoretical model for a blurry image using the image of the LS and the circle of confusion (CoC), and provide equations for the image. We experimentally investigate the proposed system and show that if the relative size of LS to its distance from the camera is less than a certain value, which is determined by the camera settings, the defocusing will increase the image size. We also show that for a larger aperture, which results in higher received power, the interference level between two LSs is increased due to defocusing.

The remainder of this paper is organized as follows. In Section II, the system model and the theoretical analysis are presented. In Section III, the experimental results and discussion is given. Finally, Section IV concludes the paper.

II. SYSTEM MODEL

Figure 1 illustrates the schematic system model. It is composed of a disc-shape LS with a diameter of a_o and a camera located at a distance of L from the LS. Note that, an aperture with a diameter of a is positioned in front of the LS in order to adjust its size. If we model the lens system of the camera with a single convex lens with a focal length f, the light source and the IS are placed at a distance of d_o and d_s from the lens,

respectively. Based on the analysis for a thin lens, the image is created at a distance d_i given as:

$$d_\mathrm{i} = \frac{d_\mathrm{o} f}{d_\mathrm{o} - f}, \tag{1}$$

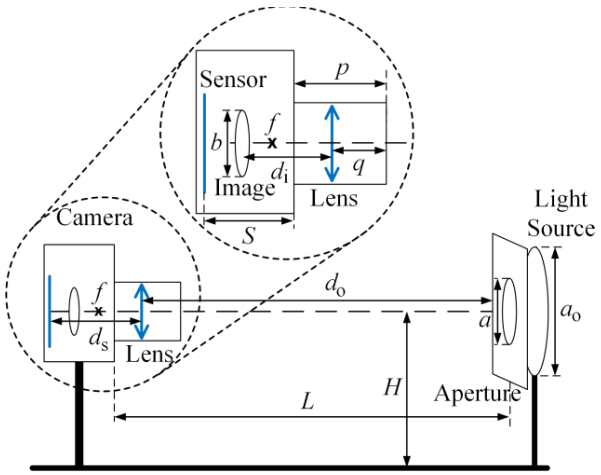

Fig. 1. Proposed system model for characteristics of defocused image.

where d_o and d_s are distances of LS and IS from the lens, respectively. The lens magnification factor $M = -\frac{b}{a} = -\frac{d_\mathrm{i}}{d_\mathrm{o}}$, where, b is the diameter of the image when the LS is in focus, and the negative sign is for an inverted image. To find the parameters of the modeled convex lens, experimentally, the LS should be in focus, i.e., $L = d_\mathrm{f}$, where d_f is the focusing distance of the lens, which we define it as the distance from the object that is in focus from the junction of camera and the lens, hence $d_\mathrm{i} = d_\mathrm{s}$. Knowing that, $d_\mathrm{o} = d_\mathrm{f} - p + q$, $d_\mathrm{s} = \frac{b d_\mathrm{o}}{a}$, and $d_\mathrm{s} = S + p - q$, where D_I is the diameter of the clear image on IS, S is the distance from the sensor to the junction of camera and the camera lens, and the distance from the position of modeled lens from the front end of the camera lens, and q can be obtained as:

$$q = \frac{aS - bd_\mathrm{f}}{a + b} + p. \tag{2}$$

Therefore, $d_\mathrm{o} = \frac{a(S+L)}{a+b}$. From (1), (2) and M we can write:

$$f = \frac{ab(d_\mathrm{f} + S)}{a^2 - b^2}. \tag{3}$$

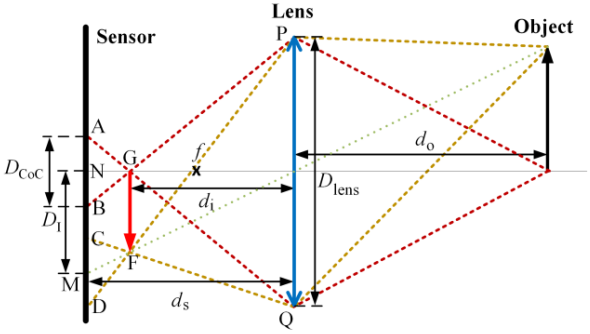

Fig. 2. The configuration of object, lens, image and sensor.

For the camera focused at a different distance, f and the position of the modeled lens will change with no image being created on the image plane, i.e., $d_\mathrm{s} \neq d_\mathrm{i}$. Therefore, no convergence of the received light beams from the object on the image plane and hence a CoC will be created for each point of the image (see Fig. 2). If the diameter of CoC > the pixel size, then the image on the camera becomes blurry.

From Fig. 2, since ΔAGB~ΔPGQ, ΔCFD~ΔPFQ, and the heights of ΔPFQ and ΔPGQ are equal, $\overline{\mathrm{AB}} = \overline{\mathrm{CD}}$. This means that defocusing works similar to a moving average filter with a window size of $\overline{\mathrm{AB}}$, R as given by:

$$I(x,y) = I_\mathrm{o}(x,y) \otimes\otimes I_\mathrm{CoC}(x,y). \tag{4}$$

where, $I_\mathrm{CoC}(x,y) = U\left(\sqrt{x^2+y^2}\right) - U\left(\sqrt{x^2+y^2} - D_\mathrm{CoC}/2\right)$ is the CoC disc function, $U(.)$ is the Heaviside step function, $I_\mathrm{o}(x,y) = h_\mathrm{I}\left(U\left(\sqrt{x^2+y^2}\right) - U\left(\sqrt{x^2+y^2} - d_\mathrm{I}/2\right)\right)$ is the intensity function of the image when LS is in focus (i.e., for a disc-shaped LS), and $\otimes\otimes$ is 2D convolution operation. Here, D_CoC is defined as:

$$D_\mathrm{CoC} = \frac{D_\mathrm{lens}}{2d_\mathrm{i}} |d_\mathrm{i} - d_\mathrm{s}|. \tag{5}$$

where $D_\mathrm{lens} = \frac{f_\mathrm{l}}{f_\mathrm{stop}}$, f_l, f_stop, d_i, and d_s denote the lens aperture diameter, camera lens focal length, f-stop of the aperture, distance from the image to the lens, and distance from the IS to the lens, respectively. Accordingly, decreasing the aperture size (AS) results in less defocusing effect. Since the output form of 2D convolution in (2) is complex, here we estimate the 2D convolution using a 1D convolution by considering the intensity of a row of blurry images of LS, which contains the diameter. Figure 3(a), (b), and (c) illustrate the intensity as a function of pixel number for the row containing the diameter of the LS, circle of confusion, and output blurry image, respectively. The proposed model can be characterized by four parameters of the maximum intensity, h, half-power full-width (HPFW) w, and left and right slopes from A to B and C to D, s_l and s_r, respectively. The normalized values of h and w are $h_\mathrm{norm} = \frac{h}{h_\mathrm{I}}$ and $w_\mathrm{norm} = \frac{w}{D_\mathrm{I}}$, where h_I is maximum intensity of the clear image on IS. For the camera sensor and the LS in line of sight configuration, the absolute value of the left and the right slopes are equal, i.e., $s_\mathrm{l} = -s_\mathrm{r}$.

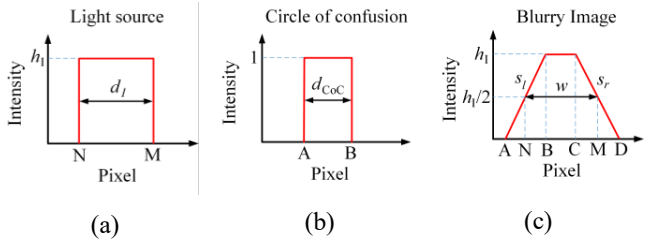

Fig. 3. The proposed model for intensity vs. pixel number for diameter of (a) light source, (b) circle of confusion, and (c) blurry image.

The normalized HPFW of the image is defined as:

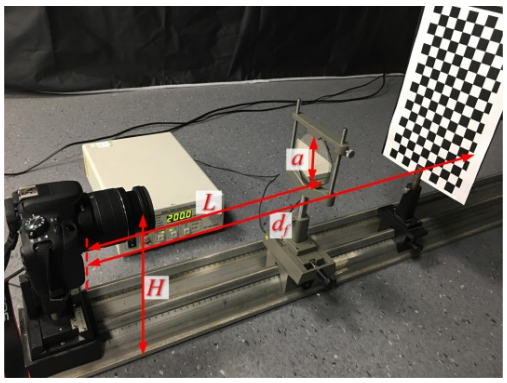

Fig. 4. Experimental system setup for evaluation of the proposed method.

$$w_{\text{norm}} = \frac{|D_{\text{CoC}} - D_{\text{I}}| + D_{\text{CoC}} + D_{\text{I}}}{2D_{\text{I}}} \tag{6}$$

Using (1) and (5), and for $d_{\text{I}} = a\frac{d_{\text{s}}}{d_{\text{o}}}$, (6) can be written as:

$$w_{\text{norm}} = \frac{|\alpha| + \alpha}{2d_{\text{s}}f} + 1 \tag{7}$$

where $\alpha = \frac{1}{a}(D_{\text{lens}}|d_{\text{o}}f - d_{\text{s}}(d_{\text{o}} - f)| - d_{\text{s}}af)$.

In C2C communications, $d_{\text{o}} \gg f$ so we have $\rho = \frac{a}{d_{\text{o}}}$ as the ratio of the size of LS to its distance from the lens and approximate $\alpha \approx \frac{1}{\rho}(D_{\text{lens}}|f - d_{\text{s}}| - d_{\text{s}}\rho f)$. Note, since the average of the intensity should remain the same, then $h_{\text{norm}} = (w_{\text{norm}})^{-1}$.The normalized slope is given as:

$$s_{\text{l,norm}} = \frac{D_{\text{I}}h_{\text{norm}}}{D_{\text{CoC}} + D_{\text{I}} - |D_{\text{CoC}} - D_{\text{I}}|} = \frac{D_{\text{I}}}{D_{\text{CoC}}} \tag{8}$$

Using (5) we have:

$$s_{\text{l,norm}} = \frac{d_{\text{s}}af}{D_{\text{lens}}|d_{\text{o}}f - d_{\text{s}}(d_{\text{o}} - f)|} \tag{8}$$

For $d_{\text{o}} \gg f$, (10) can be approximated by:

$$s_{\text{l,norm}} = \frac{d_{\text{s}}\rho f}{D_{\text{lens}}|f - d_{\text{s}}|} \tag{9}$$

For $D_{\text{CoC}} > D_{\text{I}}$, from (1) and (5), we have:

$$a < \frac{D_{\text{lens}}(d_{\text{o}} - f)^2}{d_{\text{o}}f^2}\left|\frac{d_{\text{o}}f}{d_{\text{o}} - f} - d_{\text{s}}\right| \tag{11}$$

This means that if the condition in (11) is valid then the image width due to defocusing is bigger than the size of the image when LS is in focus, hence the system may introduce crosstalk. If $d_{\text{o}} \gg f$, the condition in (11) can be approximated by:

$$\rho < \frac{D_{\text{lens}}}{f^2}|f - d_{\text{s}}| \tag{10}$$

III. Results and Discussion

Figure 4 illustrates the experimental setup for evaluation of the proposed system, composed of OSRAM CDW-031 OLED LS, circular aperture, check-board (a square size of 2×2 cm, and Canon EOS 100D (Rebel 10B) camera with an 18-55 mm lens. The height of the center of the camera, the OLED, light source aperture, and the check-board from the floor was 0.25 m. The LS aperture and the camera were in line of sight. All system key parameters are given in Table I. Figure 5 shows a flowchart for the experimental procedure. Note, the followings: (*i*) the average of 10 RAW pictures were taken to reduce the temporal noise standard deviation; (*ii*) for a clear image on the IS, the aperture size was set to the minimum (or the maximum f-stop, where in this paper it was 36) and the same procedure was employed to get the HPFW of the clear image; and (*iii*) get the slope, a 1st order polynomial curve was fitted to the curve from A to B and C to D in Fig. 3(c).

Table I. System Parameters

Parameter	Value
OLED diameter	8 cm
OLED drive current	200 mA
Height of the transmitter and camera, H	25 cm
Check-board square size	2 cm
Lens focal length, f_l	55 mm
Exposure time, T_{exp}	1/100 s
Camera RAW image resolution, $U \times V$	5184 × 3456
Sensor size	22.3 × 14.9
Bit depth of each pixel (quantization level)	14 bits
Distance from image sensor to the junction of the lens and camera, S	4 cm
Raw picture dark level intensity	2047
Camera ISO	400

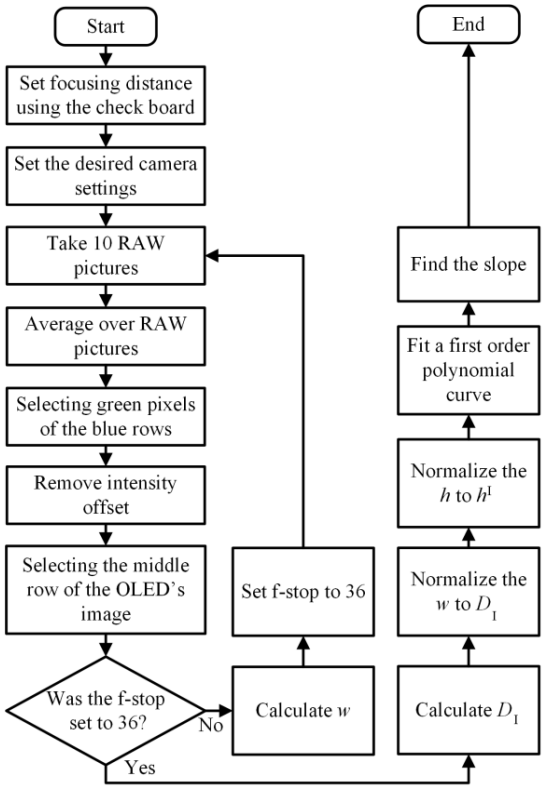

Fig. 5. Flowchart for image processing.

A. *Impact of the focusing distance*

Figures 6 (a) and (b) show the normalized intensity of the pixel vs. the normalized distance from the centre of the image for a range of f_d and the diameters of LS aperture of 0.5 and 8 cm at $L = 60$ cm. For the LS aperture diameter of 0.5 cm the condition in (11) is valid, so by defocusing the width of the image is increased. Whereas for the 8 cm diameter LS aperture the condition in (11) do not hold for any defocusing range, and therefore by defusing only the slope of the image is changed.

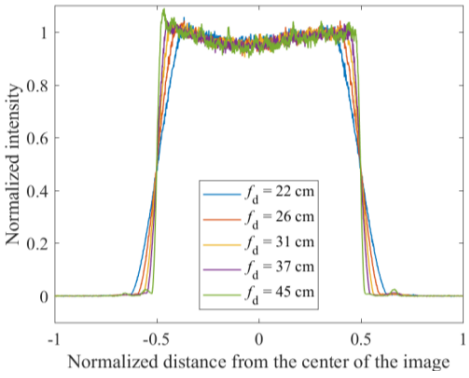

(a)

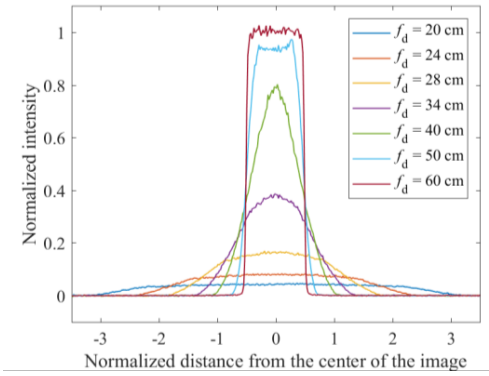

(b)

Fig. 6. Normalized intensity image vs. the normalized distance from the centre of the image for a range of f_d and $L = 60$ cm for a LS apertures of (a) 8 cm, and (b) 5 mm.

Figures 7 depict the normalized width, height, and slope of the blurred image against the focusing distance for $a = 0.5$ cm and $L = 60$ cm, $a = 8$ cm and $L = 60$ cm, and $a = 8$ cm and $L = 90$ cm and for f-stop of 5.6. Results show that for an 8 cm OLED at L of 60 and 90 cm the condition in (11) do not hold with no changes in both the height and width. At L of 60 cm, however, for a 0.5 cm OLED, the condition in (11) holds, with the width of the image becoming 5 times larger when the camera was focused at 20 cm. Also, the slope of the image is maximum at a focusing distance equal to the link span becoming 16 times larger for the 8 cm OLED compared to the 0.5 cm OLED. Note that, the slope of the image is ~1.5 times larger for $L = 60$ cm compared to $L = 90$ cm, which is in agreement with (11).

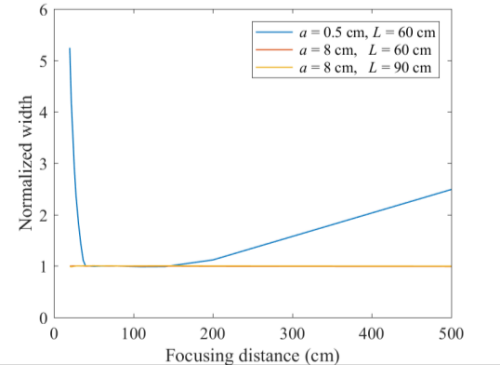

(a)

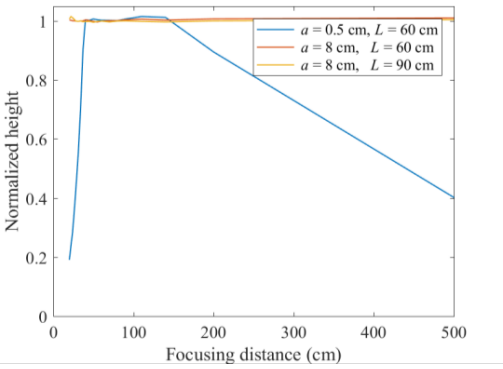

(b)

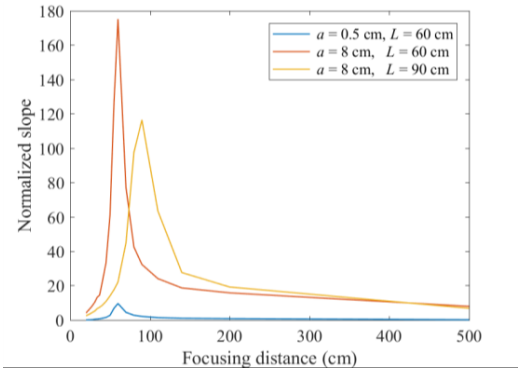

(c)

Fig. 7. Normalized values of the image of a LS vs. focusing distances for LS apertures of 0.5 cm, 8 cm, and 8 cm at L of 60 cm, 60cm and 90 cm, respectively and a lens f-stop was 5.6 for (a) width, (b) height, and (c) slope.

B. *Impact of the Link span*

Figure 8 depict the normalized width, height, and slope of the image as function of link span L for the camera focused at d_f = 20 cm and $d_f = \infty$ with a LS aperture diameter of 3 cm and an aperture f-stop of 5.6. The results show that when the camera is focused at infinity, the width and height of the image remain unity and the slope of image increases by increasing the link span. On the other hand, when the camera is focused L of 20 cm, the slope is maximum at 20 cm and decreases by increasing the link span. Besides, for a $d_f = 20$ cm, the width increases linearly beyond L of 60 cm and the height decreases proportionally to L^{-1}.

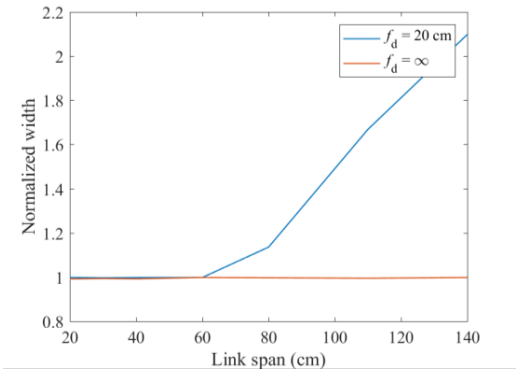

(a)

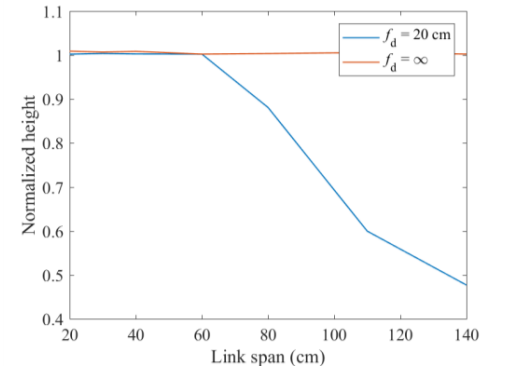

(b)

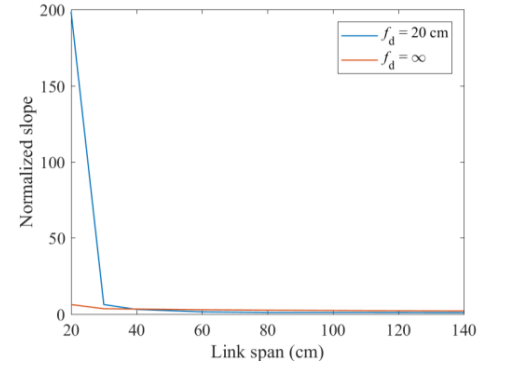

(c)

Fig. 8. Normalized parameters of the image of a LS against link span camera focused at 20 cm and infinity, the LS aperture diameter of 3 cm, and the camera lens f-stop of 5.6 for: (a) width, (b) height, and (c) slope.

IV. Conclusion

In this paper, we proposed a model for a defocused image of a light source in optical camera communications. The blurred image was characterized by four parameters of width, height, and left and right slope of the hazy area. The width of the image is important since it may introduce interference to the system with other neighboring light sources. The parameters were theoretically obtained based on light source, channel and camera parameters. The system was experimentally investigated and the results were compared to the theoretical analysis. The results showed that based on the size of the light source and the link span, the size of the blurred image of the light source due to defocusing may be larger than the focused clear image, hence a higher chance of interference. This width and the slope increased and decreased with the with the link span, respectively.

Acknowledgment

This work is supported by the European Union's Horizon 2020 research and innovation programme under the Marie Slodowska-Curie grant agreement no 764461 (VISION) and the EPSRC research grant EP/P006280/1: MARVEL and under the Marie Slodowska-Curie ITN grant no. 764461 MARVEL.

References

[1] R. X. Ferreira, E. Xie, J. J. McKendry, S. Rajbhandari, H. Chun, G. Faulkner, *et al.*, "High bandwidth GaN-based micro-LEDs for multi-Gb/s visible light communications," *IEEE Photonics Technology Letters,* vol. 28, pp. 2023-2026, 2016.

[2] Z. Ghassemlooy, L. N. Alves, S. Zvanovec, and M.-A. Khalighi, *Visible Light Communications: Theory and Applications*: CRC Press, 2017.

[3] H. Chinthaka, N. Premachandra, T. Yendo, T. Yamasato, T. Fujii, M. Tanimoto, *et al.*, "Detection of LED traffic light by image processing for visible light communication system," in *Intelligent Vehicles Symposium, 2009 IEEE*, 2009, pp. 179-184.

[4] Y. Kawai, T. Yamazato, H. Okada, T. Fujii, T. Yendo, S. Arai, *et al.*, "Tracking of LED headlights considering NLOS for an image sensor based V2I-VLC," in *International Conference and Exhibition on Visible Light Communications*, 2015.

[5] N. Bani Hassan, Z. Ghassemlooy, S. Zvanovec, P. Luo, and H. Le Minh, "Non-line-of-sight 2 × N indoor optical camera communications," *Applied Optics,* vol. 57, pp. 1-6, 2017.

[6] S. Hranilovic and F. R. Kschischang, "Short-range wireless optical communication using pixilated transmitters and imaging receivers," in *Communications, 2004 IEEE International Conference on*, 2004, pp. 891-895.

[7] P. Luo, M. Zhang, Z. Ghassemlooy, H. Le Minh, H.-M. Tsai, X. Tang, *et al.*, "Experimental demonstration of RGB LED-based optical camera communications," *IEEE Photonics Journal,* vol. 7, pp. 1-12, 2015.

[8] P. H. Pathak, X. Feng, P. Hu, and P. Mohapatra, "Visible light communication, networking, and sensing: A survey, potential and challenges," *ieee communications surveys & tutorials,* vol. 17, pp. 2047-2077, 2015.

[9] C. Danakis, M. Afgani, G. Povey, I. Underwood, and H. Haas, "Using a CMOS camera sensor for visible light communication," in *Globecom Workshops (GC Wkshps), 2012 IEEE*, 2012, pp. 1244-1248.

[10] Sony. *Sony xperia xz premium*. Available: https://www.sonymobile.com/gb/products/phones/xperia-xz-premium/specifications

[11] Phantom. *Phantom v2512*. Available: http://www.phantomhighspeed.com/Products/Ultrahigh-Speed-Cameras/v2512

[12] P. Luo, Z. Ghassemlooy, H. Le Minh, X. Tang, and H.-M. Tsai, "Undersampled phase shift ON-OFF keying for camera communication," in *Wireless Communications and Signal Processing (WCSP), 2014 Sixth International Conference on*, 2014, pp. 1-6.

[13] R. D. Roberts, "Undersampled frequency shift ON-OFF keying (UFSOOK) for camera communications (CamCom)," in *Wireless and Optical Communication Conference (WOCC), 2013 22nd*, 2013, pp. 645-648.

[14] T. Nagura, T. Yamazato, M. Katayama, T. Yendo, T. Fujii, and H. Okada, "Tracking an LED array transmitter for visible light communications in the driving situation," in *Wireless Communication Systems (ISWCS), 2010 7th International Symposium on*, 2010, pp. 765-769.

[15] T. Yamazato, I. Takai, H. Okada, T. Fujii, T. Yendo, S. Arai, *et al.*, "Image-sensor-based visible light communication for automotive applications," *IEEE Communications Magazine,* vol. 52, pp. 88-97, 2014.